01 Jan 2023

High Temperature Confocal Scanning Laser Microscopy Analysis of Dead-Burned Magnesia Aggregates

Tyler Richards

Viraj Athavale

Jeffrey D. Smith
Missouri University of Science and Technology, jsmith@mst.edu

Ronald J. O'Malley
Missouri University of Science and Technology, omalleyr@mst.edu

Recommended Citation

T. Richards et al., "High Temperature Confocal Scanning Laser Microscopy Analysis of Dead-Burned Magnesia Aggregates," *International Journal of Ceramic Engineering and Science*, Wiley Open Access, Jan 2023.
The definitive version is available at https://doi.org/10.1002/ces2.10175

Received: 29 January 2023 | Accepted: 7 April 2023

DOI: 10.1002/ces2.10175

International Journal of Ceramic Engineering & Science

RESEARCH ARTICLE

High temperature confocal scanning laser microscopy analysis of dead-burned magnesia aggregates

Tyler Richards | **Viraj Athavale** | **Jeffrey Smith** | **Ronald O'Malley**

Department of Materials Science and Engineering, Missouri University of Science and Technology, Rolla, Missouri, USA

Correspondence
Tyler Richards, Missouri University of Science and Technology, 1400 N. Bishop Ave., Rolla, MO 65401, USA.
Email: tmr27f@mst.edu

Abstract

Dead-burned magnesia is a commonly used material in the manufacturing of refractories for the steelmaking industry. Aggregates of dead-burned magnesia contain secondary phases due to the impurities within the magnesite rock used in its production. While these phases can aid in sintering magnesia, they may have some impact on the high-temperature performance of the refractory product. High-temperature confocal scanning laser microscopy was utilized to observe the behavior of dead-burned magnesia aggregates at elevated temperatures (up to 1550°C). Liquid formation was detected even at temperatures below 1350°C. In some cases, this liquid quickly exuded from the aggregate surface. This liquid phase was characterized through microscopy and chemical analysis to determine the impact of impurity content on the formation and behavior of this liquid phase, and conclusions are drawn on its detrimental impact on the material's refractoriness in a steelmaking environment.

KEYWORDS
impurities, magnesium oxide, microscopy, refractories

1 | INTRODUCTION

Dead-burned magnesia is a material commonly used in refractories. Dead-burned magnesia is produced by calcining magnesite ($MgCO_3$). The final product can vary depending on the type of magnesite used and where it originated from. McDowell and Howe[1] describe two main types of magnesite: "crystalline" and "amorphous" (in reality, coarse and fine grained, respectively). Magnesite rock will often contain some amount of impurities, often iron oxide, calcium oxide, and silicate-based compounds. "Crystalline" magnesite is often higher in Fe or Ca-based oxide/carbonate impurities, whereas "amorphous" magnesite will contain more silicate-based impurities. Upon calcination, CO_2 is driven off, resulting in an approximate 50% reduction in weight. At sufficiently high temperatures, the particles will also sinter, reducing volume and increasing density, thereby increasing resistance to hydration by moisture in the air. The temperature necessary for this sintering to occur depends on the impurity content of the magnesite, ranging from 1450 to 1700°C depending on the iron oxide content. Higher iron oxide content (McDowell and Howe suggest up to 8% Fe_2O_3) may be desirable for decreasing the sintering temperature but may also have a negative impact on high-temperature performance as it lowers the melting temperature of the magnesia (by forming a magnesioferritic solid solution).[2] The microstructure of the dead-burned magnesia consists of periclase (MgO)

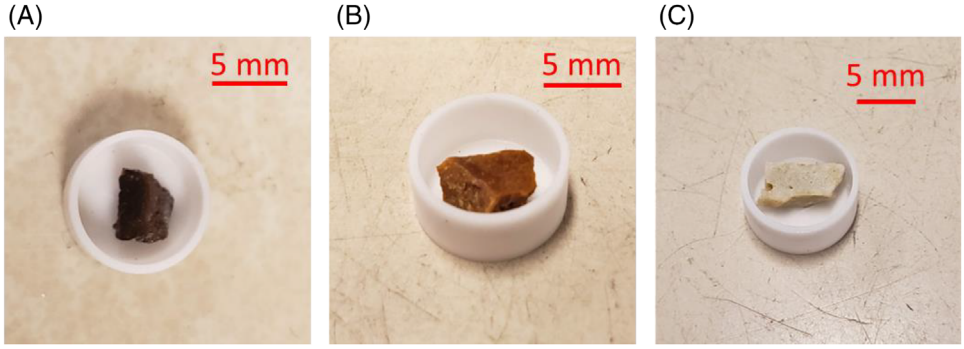

FIGURE 1 Aggregates used for confocal microscopy study (A: "dark", B: "medium", C: "light"). A 9-mm diameter alumina crucible was used for containment.

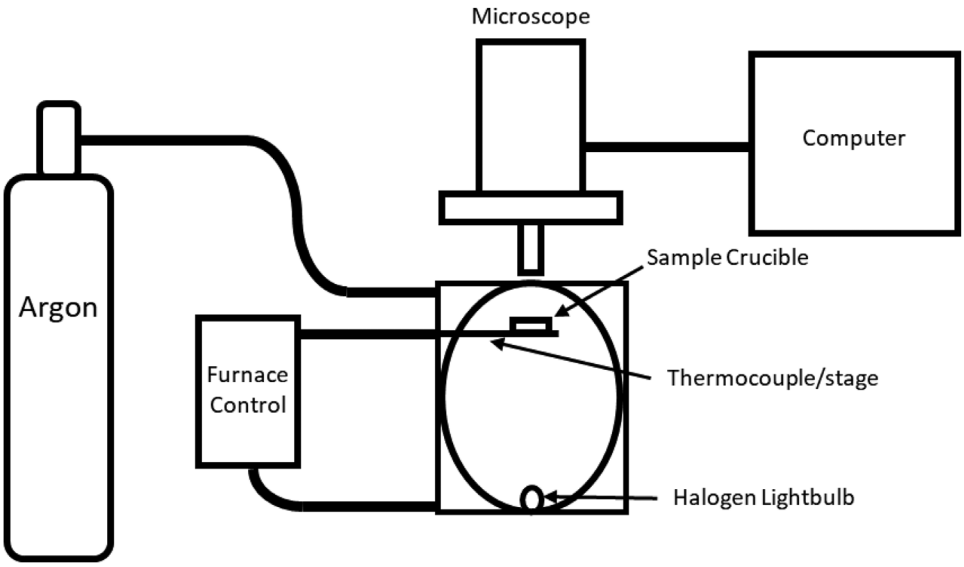

FIGURE 2 Schematic representation of the high-temperature confocal scanning laser microscope.

crystallites bound together by a secondary phase resulting from the other impurities found in the magnesite. Depending on the calcium and silicon content, a variety of phases can be found, such as orthosilicates like forsterite (Mg_2SiO_4) and monticellite ($CaMgSiO_4$).

One product in which dead-burned magnesia is commonly found is in the lining of a tundish used for continuously casting steel. The tundish is a vessel, which serves as an intermediate step between the ladle and the mold. This allows for the uninterrupted flow of steel to the mold as the emptied ladle is switched out with a full ladle. In basic steelmaking practices, MgO is an important refractory material as it is compatible with the basic fluxes that are used to cover the steel melt. This flux is a liquid oxide slag that serves as a thermal insulator, prevents oxygen and nitrogen in the air from dissolving into the melt, and can dissolve Al_2O_3 inclusions from the steel. Depending on the grade of steel being cast, the tundish lining may experience temperatures upwards of 1550 to 1680°C.

The performance of the tundish lining is critical to the efficiency of the steelmaking process and the quality of the final product. The performance of the refractory can be evaluated through its interactions with both flux and molten steel. While generally considered to be compatible with basic flux (especially compared to materials such as alumina), there are still concerns regarding the corrosion behavior of the refractory. Postmortem analysis performed by Moshtaghioun and Monshi[3] revealed the formation of low-melting temperature phases such as merwinite ($Ca_3MgSi_2O_8$) and diopside ($CaMgSi_2O_6$). These phases can cause the dissolution of MgO and are the result of interactions between infiltrating flux and the secondary phases in the dead-burned magnesia. Another concern of steelmakers, especially those who use aluminum for

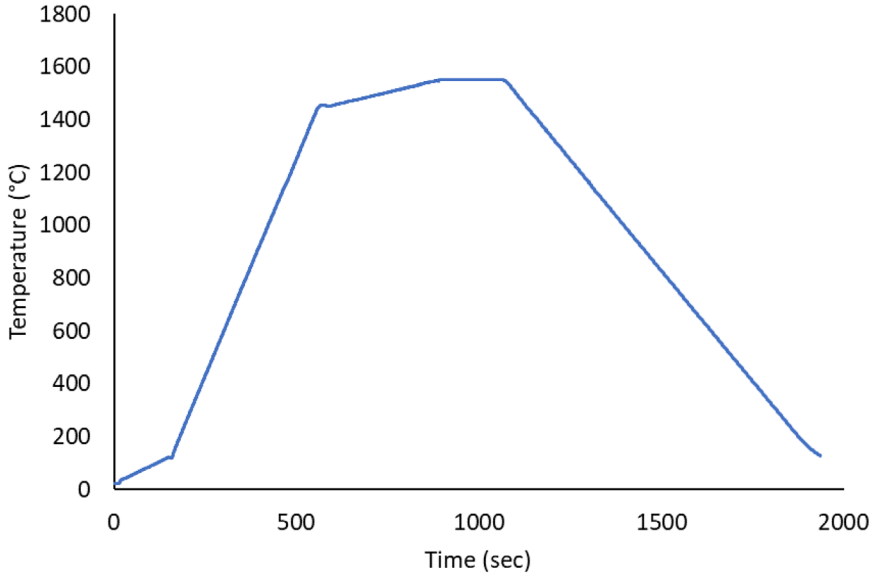

FIGURE 3 The heating schedule for the confocal laser scanning microscopy experiments.

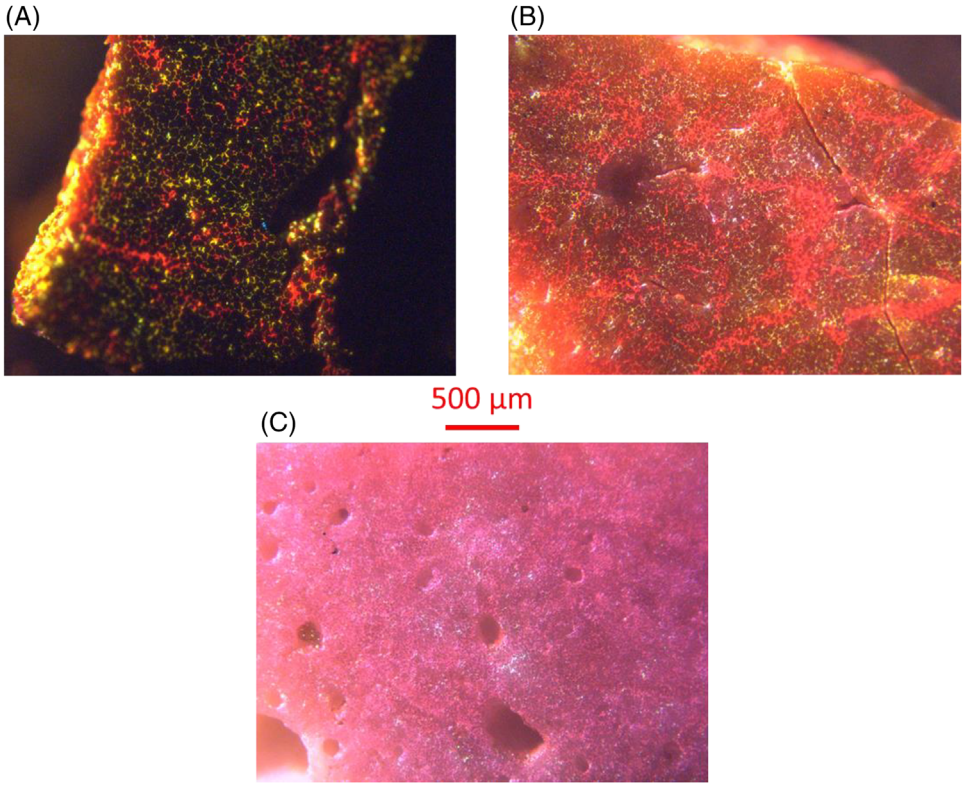

FIGURE 4 Cathodoluminescence imagery of the aggregate samples prior to confocal scanning laser microscopy experiments (A: dark, B: medium, C: light).

deoxidation of their steel, is the formation of spinel ($MgAl_2O_4$). Magnesia from the refractory may react with alumina-based inclusions in the steel to transform them into spinel.[4–6] Spinel inclusions are solid at steelmaking temperatures and are large in size, which can have a detrimental effect on the mechanical properties of the final steel product. Multiple reaction models have been suggested for how magnesia reacts with alumina to form spinel in steel,[6–8] but the specific mechanism at play may depend on the mechanism by which magnesia is transported to alumina in the steel.

For both corrosion behavior and spinel generation, the underlying mechanisms may be influenced by the secondary phases found in the dead-burned magnesia

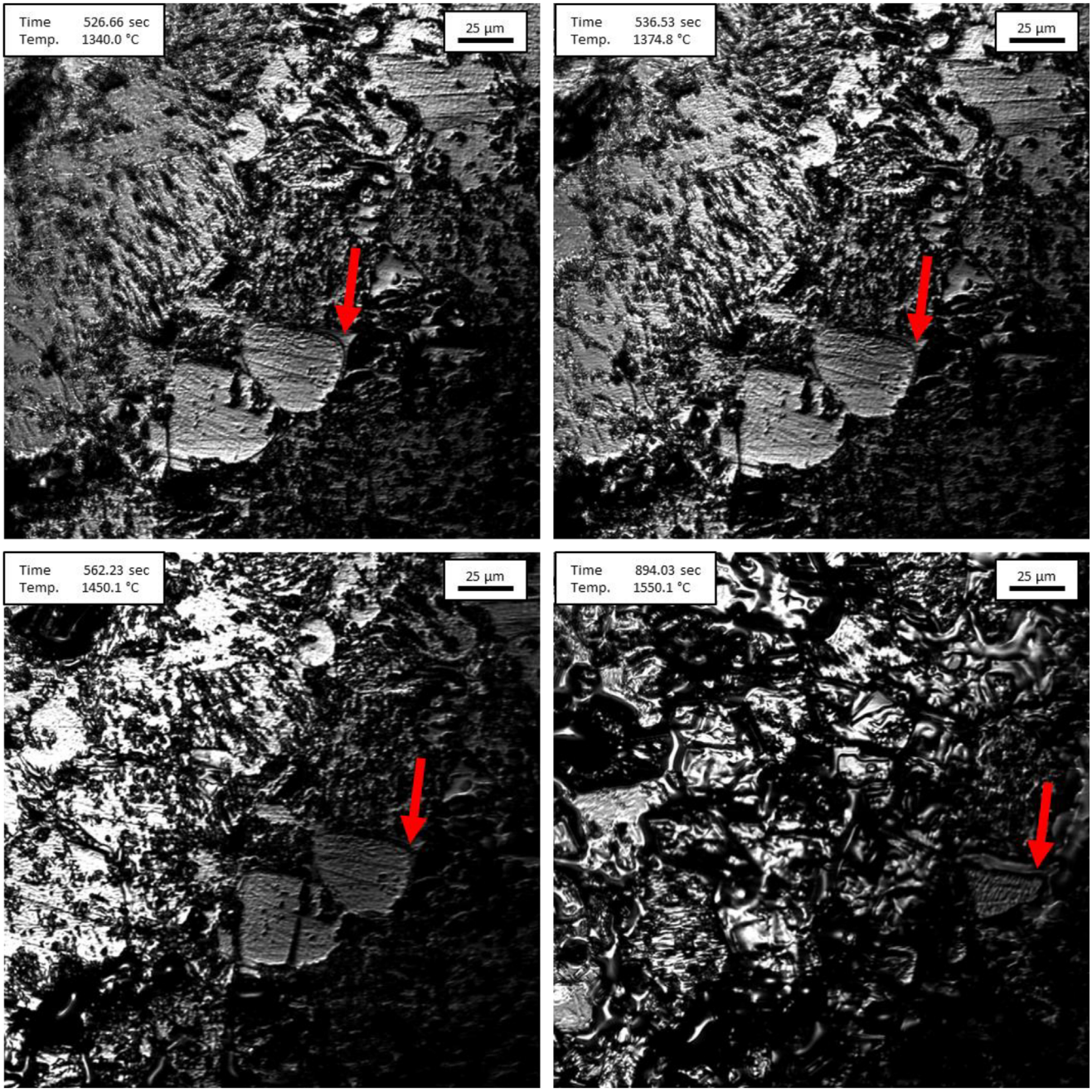

FIGURE 5 Select images taken from the confocal scanning laser microscopy experiment on the dark aggregate. The red arrow serves as a reference point for comparing images at different times/temperatures.

aggregates that result from the impurities in the original magnesite material. For example, monticellite, one of the possible orthosilicates found in dead-burned magnesia, on its own has a melting temperature of 1498°C, which is lower than the temperature of some steel melts. If this phase is to melt during the steelmaking process, that could contribute to the formation of the previously described low-melting temperature phases. The purpose of this work is to perform in situ observation of dead-burned magnesia at elevated temperatures through the use of a confocal scanning laser microscope. In doing so, the behavior of the secondary phases can be assessed and discussed as a critical aspect of the refractory material's performance.

2 | EXPERIMENTAL PROCEDURE

Dead-burned magnesia aggregates were received from a refractory manufacturer that produces MgO-based tundish lining materials. The aggregates were on the order of 15 mm in diameter. These aggregates are typically crushed into smaller aggregates before batching the material for the

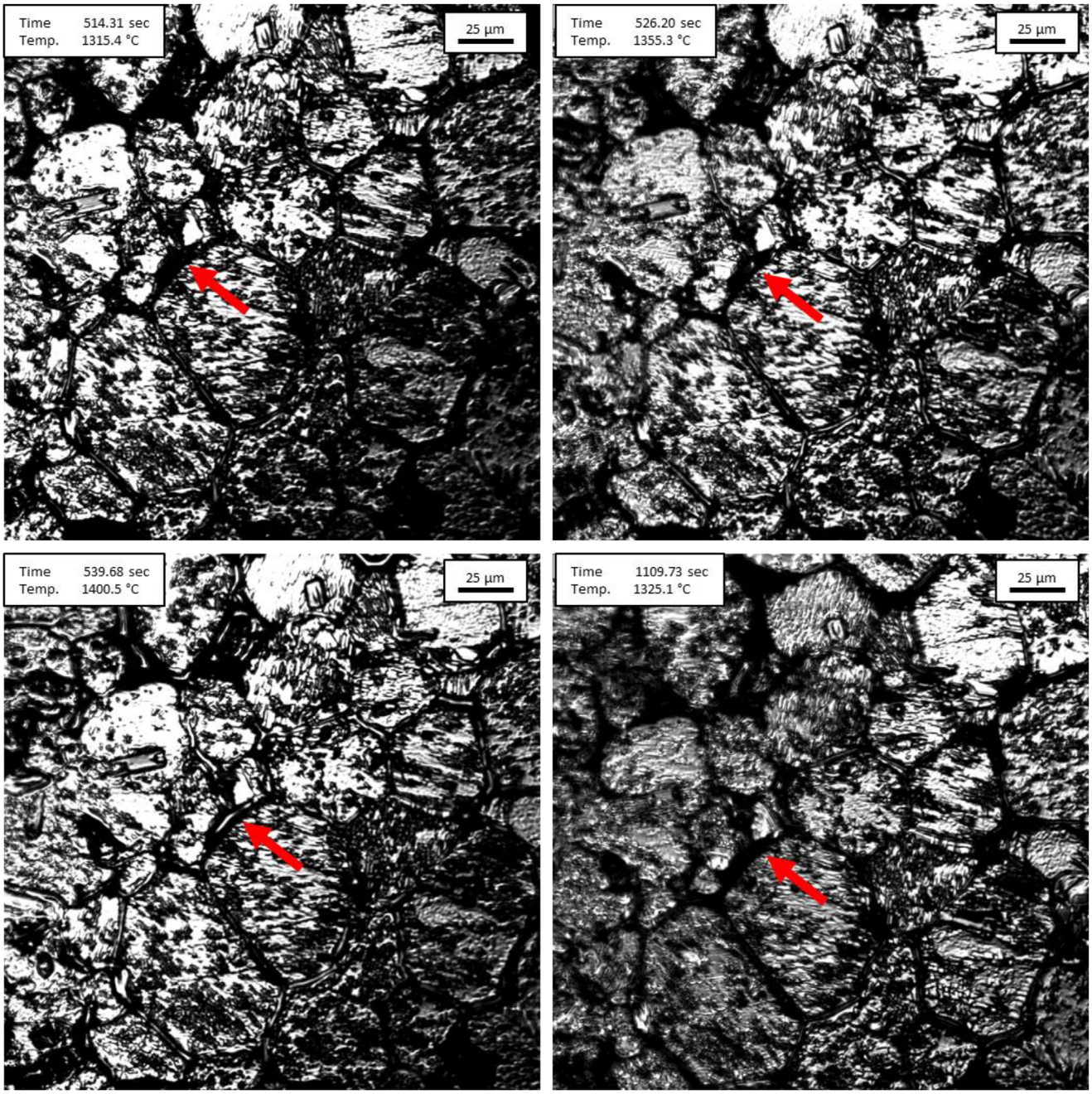

FIGURE 6 Select images taken from the second confocal scanning laser microscopy experiment on the dark aggregate.

final product. The aggregates were hand-polished on one side to produce a smooth surface. Resin-embedded diamond grinding and polishing pads (220 grit through 4000 grit) were used in addition to 3- and 1-µm diamond suspension applied to cloth pads. Figure 1 shows images of the aggregates after polishing. Within the batch of dead-burned magnesia aggregates was a variety of aggregate compositions. Each consisted of MgO crystallites bonded by Ca-Mg-Si oxide-based secondary phases, but the exact composition of such secondary phases and the impurity level of the MgO (i.e., Fe content) varies depending on the source of the individual aggregate. For the purposes of this paper, the samples will be labeled dark, medium, and light, referring to the color of the aggregate.

To first characterize the samples, cathodoluminescence (CL) was used to identify the presence of the secondary phases. CL is a microscopy technique that employs a diffuse beam of electrons that induce luminescence in certain materials, causing the emission of photons in the visible light spectrum. The colors observed depend on the chemistry of the sample and can even be influenced by the concentration and type of trace impurities in the sample.

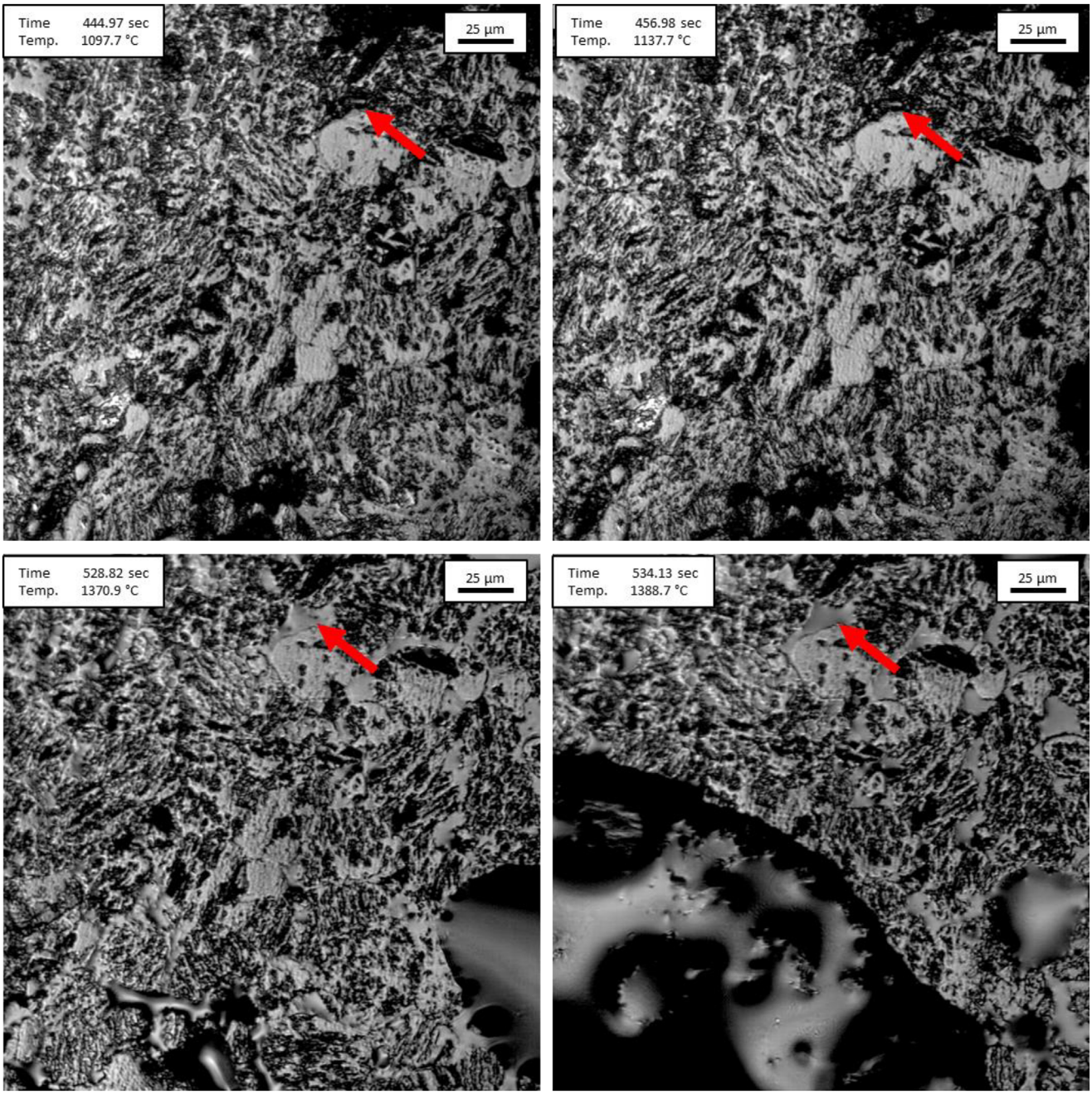

FIGURE 7 Select images taken from the confocal scanning laser microscopy experiment on the medium aggregate. The red arrow serves as a reference point for comparing images at different times/temperatures.

Therefore, this technique is beneficial for rapidly distinguishing phases with stark contrast that is apparent even to the naked eye. The results of CL also helped identify reference points to use for laser confocal and scanning electron microscopy.

In order to identify what secondary phases would be present in the aggregates, X-ray diffraction (XRD) was employed on a random selection of aggregates from the provided batch. While the nature of the sample would make it difficult to quantify each phase accurately, the results of the XRD analysis are still useful in identifying the possible eutectics within the overall system.

A high-temperature scanning laser confocal microscope was used to observe each sample individually at elevated temperatures. A schematic of the equipment is shown in Figure 2. The sample is placed in a 9-mm diameter alumina crucible and then placed on a platinum sample holder inside the furnace chamber. A thermocouple wire is incorporated into the Pt sample holder to record and maintain temperatures throughout the experiment. Heat is provided

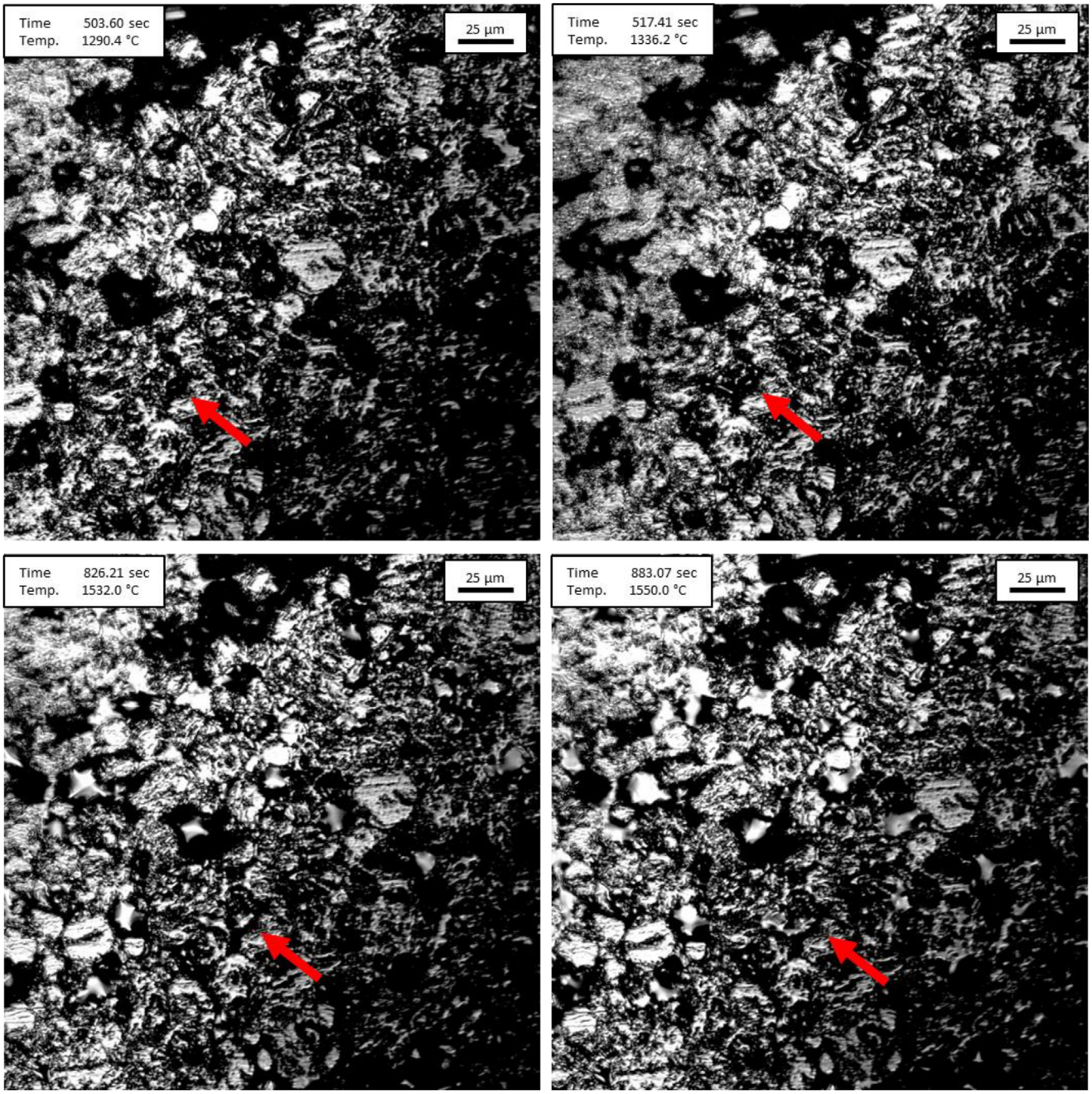

FIGURE 8 Select images taken from the confocal scanning laser microscopy experiment on the light aggregate. The red arrow serves as a reference point for comparing images at different times/temperatures.

by a halogen bulb. The curved shape of the gold-plated inner chamber wall aides in focusing the heat generated by the lamp on the sample. A quartz viewport allows for observation of the sample. A laser was scanned across the sample surface to generate the image. By use of a laser, as opposed to diffuse light as typically seen in optical microscopes, imaging can be performed at higher magnification compared to typical optical microscopy. Additionally, scanning laser confocal microscopy allows for clear images that are not as easily impacted by blackbody radiation at elevated temperatures that might make optical observation otherwise difficult.

The furnace chamber was repeatedly evacuated and refilled with ultra-high purity Argon gas, which was passed through two filter gas train systems. Three cycles of 3-min duration and the use of filters ensured the removal of any trace oxygen. This procedure also reduced the presence of gaseous impurities inside the chamber.

The heat schedule used for the experiment is represented in Figure 3. The temperature was initially raised

to 120°C at a rate of 60°C/min as a preheating step. After holding for 10 s, the temperature was then raised to 1450°C at 200°C/min. The ramp rate was chosen such as to prevent the crucible cracking from excessive heat. The sample was held at this temperature for 30 s, then raised to 1550°C at a rate of 20°C/min. This step was added as the phases typically seen in these types of aggregates have melting points within this range (for example, monticellite has a melting point of 1498°C). After holding at 1550°C for 180 s, the sample was cooled down to 100°C at a rate of 100°C/min, then allowed to cool to room temperature naturally. For the duration of the experiment, Ar gas was flowed with a recommended flow rate of 150 mL/min through the chamber. Images were taken at a rate of five frames per second during the experiment starting at 500°C on ramping up.

After the experiment was concluded, the tested sample was observed under CL again to qualitatively identify any changes in morphology or chemistry (which would be indicated by changes in color). Then, the samples were analyzed through the use of scanning electron microscopy (SEM) and energy-dispersive spectroscopy (EDS). This allowed for the chemical characterization of the phases of interest that were previously identified through CL observations. The aggregate samples were sputter coated with gold/palladium alloy to prevent charging while in the SEM.

3 | RESULTS AND DISCUSSION

Figure 4 shows CL imagery of each aggregate sample tested. In all three samples, three main phases are detected. The first is found in the dark, round particles on the order of 25–50 μm that are distributed throughout the entire aggregate. This corresponds to the crystalline MgO phase, which constitutes the majority of the aggregate by mass. These particles may luminesce a violet color, but they do not typically luminesce as bright as the other phases present, hence the relatively dark appearance. The other two phases found in each sample correspond to the secondary phases that bind the MgO crystallites together. The exact colors differ between samples, especially when comparing the Dark and Medium aggregates to the Light aggregate, due to slight variations in chemistry. The yellow phase found in the Dark and Medium aggregates has been demonstrated in previous work[9] to correspond to a calcium magnesium silicate phase with a chemistry congruent with monticellite ($CaMgSiO_4$). The orange phase typically corresponds to a phase lower in calcium and closer to forsterite (Mg_2SiO_4) in composition. In the light aggregate, the "calcium-rich" and "calcium-depleted" phases appeared white and pink, respectively. The forsteritic phase was much more prevalent in the light aggregate compared to the other samples. The relatively higher SiO_2 and lower CaO content, in addition to the light coloration and smaller periclase crystallite sizes (roughly half that of the darker aggregates) suggest this was of the variety produced from "amorphous" magnesite (again, fine-grained in reality), whereas the darker aggregates with higher calcium content were produced from "crystalline" magnesite.

TABLE 1 Summary of temperatures where liquid was first observed in each sample.

Sample	Initial liquid temperature (°C)
Dark	1350
Medium	1150
Light	1300

Figure 5 shows a selection of confocal laser scanning microscopy images taken while heating the Dark aggregate. Liquid was found to form before the initially programmed hold temperature of 1450°C. At approximately 1350°C, some movement is detected in the porosity of the aggregate, indicating the start of liquid formation. Over time, as the temperature continued to increase, liquid is observed to exude from the polished surface of the aggregate in much greater quantity. Liquid continued to exude as the temperature rose past 1450°C and up to 1550°C.

Inspection of the Dark sample before removal from the sample chamber revealed an area where the boundaries between the MgO crystallites were more pronounced (Figure 6). By reheating the sample and focusing the microscope on this region, the exuding nature of the liquid phase is more pronounced: as the temperature raised above 1325°C, liquid could be seen seeping out of the boundaries, and as the temperature decreased, the liquid could be seen retreating back into the boundaries. This demonstrated the mobility of the liquid phase at elevated temperatures.

Figure 7 shows a selection of confocal laser scanning microscopy images taken while heating the medium aggregate. Initial liquid formation was detected at approximately 1150°C. As the temperature rose past 1350°C, the liquid phase rapidly filled large pores and even spilled out across the polished surface of the aggregate.

Figure 8 shows a selection of confocal laser scanning microscopy images taken while heating the Light aggregate. Initial liquid formation was detected at approximately 1300°C. Compared to the dark and medium aggregates, the liquid did not exude onto the surface of the sample as rapidly or dramatically, typically staying within the crystallite boundaries. Table 1 summarizes the initial liquid detection temperatures across all three samples for reference.

CL imagery of the samples after heating is shown in Figure 9. In the dark and medium aggregates, orange

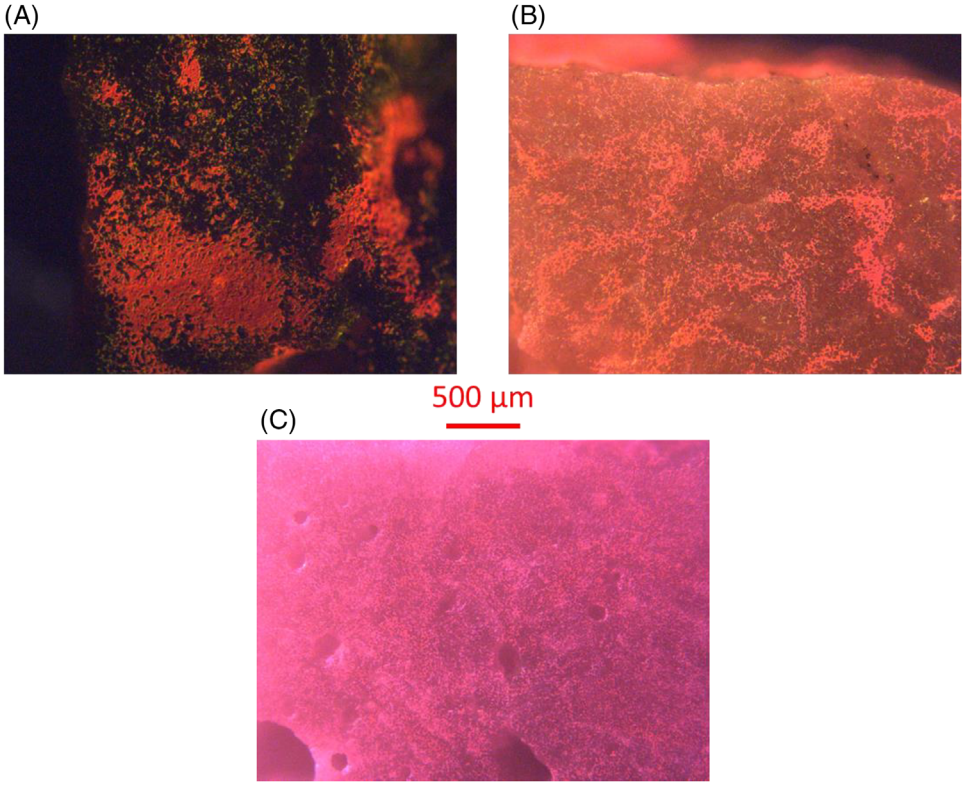

FIGURE 9 Cathodoluminescence imagery of the aggregate samples after the confocal scanning laser microscopy experiments has been conducted (A: dark, B: medium, C: light).

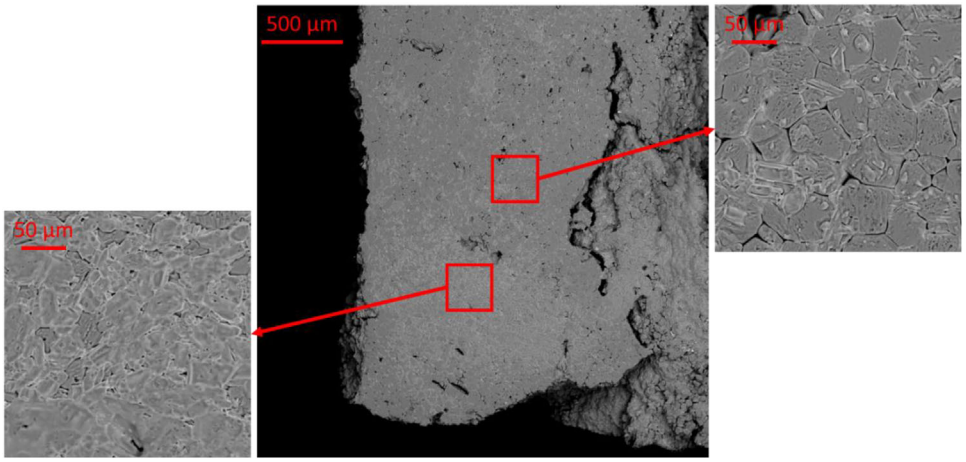

FIGURE 10 Backscattered electron imagery of the Dark aggregate.

"blotches" are found to cover portions of the MgO crystallites. The yellow phase is still observed between crystallites. Overall, the CL response appears dimmer when compared to the images shown in Figure 4. In the Light aggregate, minimal change is observed in the morphology of the sample, but the colors are again dimmer.

Backscattered electron imagery of the Dark aggregate is shown in Figure 10. The orange blotches found in Figure 9 correspond to a phase that exuded over the surface of the aggregate. In the microstructure, this phase has an almost amorphous or nanocrystalline appearance; however, in regions where less of this phase was found, it appears as oblong, angular formations, suggesting crystallinity. EDS mapping (Figure 11) indicates that the orange phase is predominately a magnesium silicate-based phase, whereas most of the calcium is found in small pockets

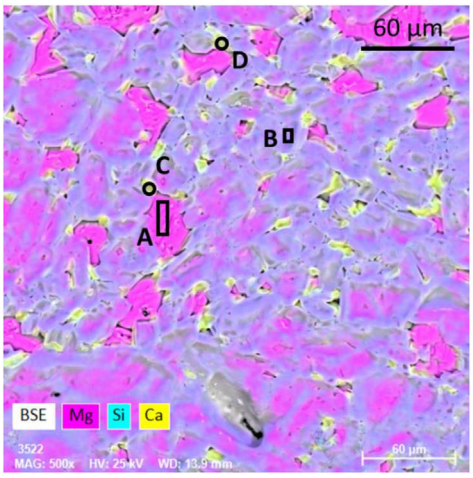

Spectrum	O	Mg	Al	Si	Ca	Fe
A	17	70				12
B	21	35		31	6	6
C	17	23	1	27	26	6
D	7	14	1	19	53	7

FIGURE 11 Energy-dispersive spectroscopy (EDS) mapping and analysis of the dark aggregate. The circles indicate the location of EDS point analysis. The boxes indicate EDS spectra were acquired over the area.

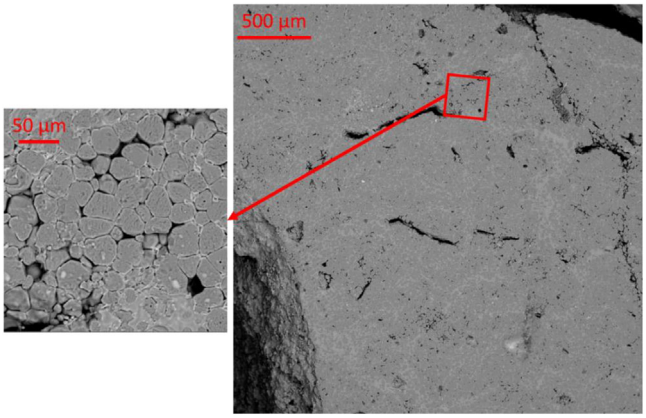

FIGURE 12 Backscattered electron imagery of the medium aggregate.

between crystallites. Point analysis indicates the same, with some variability in the calcium content. Due to the interaction volume of the electron beam, it is difficult to determine if this variability is real, or if some of the measurements were confounded by neighboring phases. The presence of iron and aluminum was also detected. Iron can often be found in solid solution with MgO in such aggregates, forming magnesiowüstite ((Mg,Fe)O). The aluminum was primarily detected in trace amounts in the secondary phases.

The Medium aggregate displayed similar results in SEM/EDS (Figures 12 and 13). The main difference between the aggregates appears to be the measured quantity of iron. In the light aggregate, SEM, and EDS results (Figures 14 and 15, respectively) support the in situ confocal laser scanning microscopy observations in that the secondary phase (which in this case is predominately the magnesium silicate-based phase) does not appear to have exuded onto the surface of the aggregate, remaining in between the crystallite boundaries. Another notable observation in the Light aggregate is the presence of aluminum-rich portions of the aggregate, possibly even forming spinel. Aluminum was also found in some of the crystallites.

In order to determine what may have caused the different behaviors within the aggregate samples, XRD was used on randomly selected untreated aggregates to determine what phases might be present. Figure 16 shows the spectra of unused light and dark periclase samples. In the light XRD sample, forsterite was the only secondary phase detected. This is congruent with the CL observations (Figures 4C and 9C) and EDS analysis (Figure 15) of the light confocal sample where a magnesium silicate-based material constituted the majority of the secondary phase. In the dark periclase sample, monticellite ($CaMgSiO_4$) was the secondary phase. This corresponds to the yellow phase detected in CL (see Figure 4A,B). In reality, it is possible that both phases may be found in each aggregate but make up a small portion of the sample and are difficult to measure. Based on these observations, it appears that, while all samples tested in the confocal scanning laser microscope did form a liquid phase at elevated temperatures, the presence of calcium-based phases may influence the fluidity of that phase. The impact on melting temperature is not as immediately obvious, as the temperature at which the first liquid was detected varied greatly between samples regardless of whether monticellite was present or not. Additionally, impurities that are in solution with the crystalline phases, such as iron and aluminum, were not indicated by XRD.

The crystalline phases identified by XRD are not sufficient on their own to explain the formation of liquid. The CaO-MgO-SiO_2 ternary system has been studied by

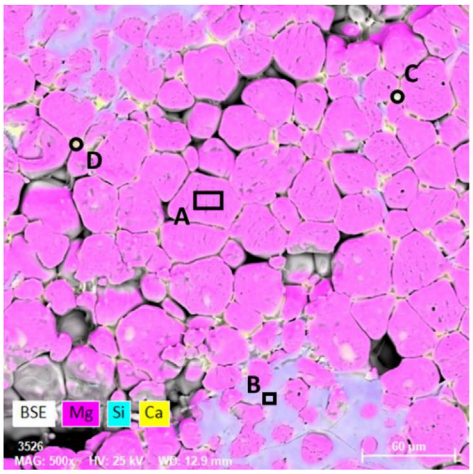

Spectrum	O	Mg	Al	Si	Ca	Fe
A	22	75				3
B	26	34		34	6	1
C	26	24		26	24	
D	14	18	1	7	58	1

FIGURE 13 Energy-dispersive spectroscopy (EDS) mapping and analysis of the medium aggregate. The circles indicate the location of EDS point analysis. The boxes indicate EDS spectra were acquired over the area.

FIGURE 14 Backscattered electron imagery of the light aggregate.

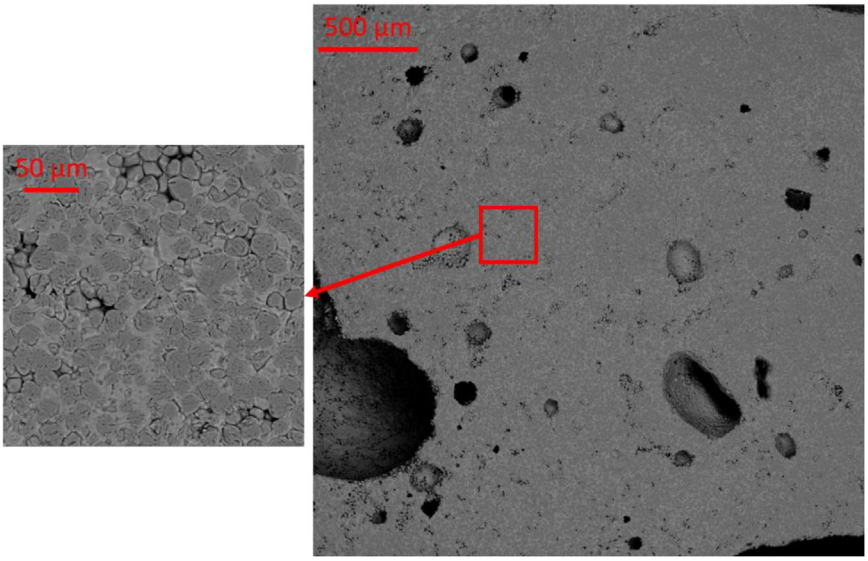

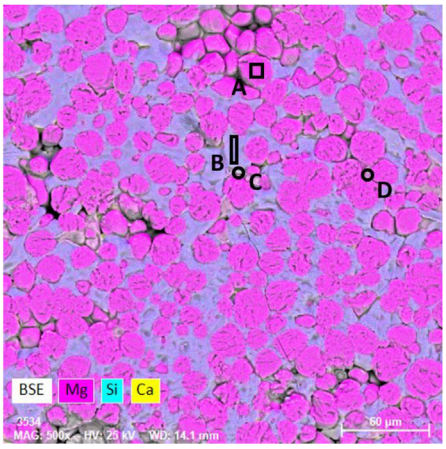

Spectrum	O	Mg	Al	Si	Ca	Ti	Fe
A	24	72	2				2
B	26	34	1	36	3		
C	30	30	2	23	14	1	1
D	26	20	50			2	1

FIGURE 15 Energy-dispersive spectroscopy (EDS) mapping and analysis of the light aggregate. The circles indicate the location of EDS point analysis. The boxes indicate EDS spectra were acquired over the area.

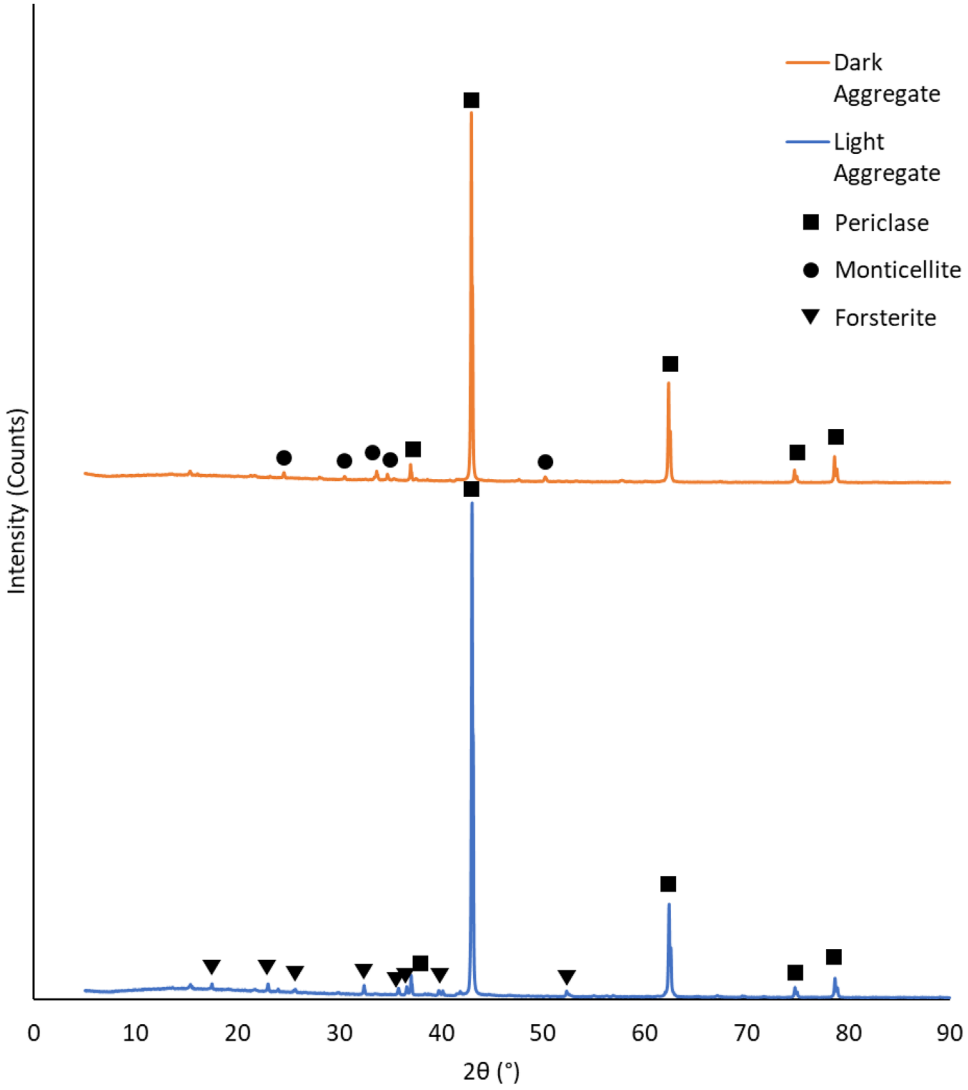

FIGURE 16 X-ray diffraction of two periclase aggregates.

multiple researchers. A phase diagram for this system is shown in Figure 17.[10] Periclase, monticellite, and forsterite form a peritectic reaction at 1502°C. Ricker and Osborn[10] studied compositions along the Alkemade line between monticellite and forsterite and did find evidence of liquid formation at temperatures as low as 1487°C, and found that in compositions within the $CaMgSiO_4$-Mg_2SiO_4-Ca_2MgSiO_7 ternary (monticellite-forsterite-akermanite) liquid may form at temperatures as low as 1430°C The lowest possible invariant point in the CaO-MgO-SiO_2 system is approximately 1320°C, between SiO_2, wollastonite ($CaSiO_3$), and diopside ($CaMgSi_2O_6$), none of which are found in the periclase aggregates. Therefore, the impurities within the aggregates must also be considered. For example, the aluminum observed in the Light aggregate may play a role in reducing melting temperatures. Biggar and O'Hara[11] studied the melting behavior of the forsterite, monticellite, spinel ($MgAl_2O_4$), and periclase system, reporting a melting temperature as low as 1425°C, and within the monticellite, spinel, periclase, and merwinite ($Ca_3MgSi_2O_8$) system a melting temperature as low as 1410°C was observed. Iron, found in all three aggregates tested, may also play a role. Chuang et al.[12] studied the effect of FeO content on the melting temperature of slags in the CaO-SiO_2-MgO-Al_2O_3 system and found that the melting temperature for multiple compositions of slags is reduced with increasing FeO content up to 20 wt%. The materials explored in the current work reside in a different section of the CaO-MgO-SiO_2-FeO quaternary, which may need further exploration.

The liquid phase generated was observed to exude from the surface of two of the three aggregates tested. As these aggregates are used for refractories used in a steelmaking environment, the impact of this liquid should be considered. In experiments and post-mortem analysis with dead-burned magnesia-containing tundish lining refractories

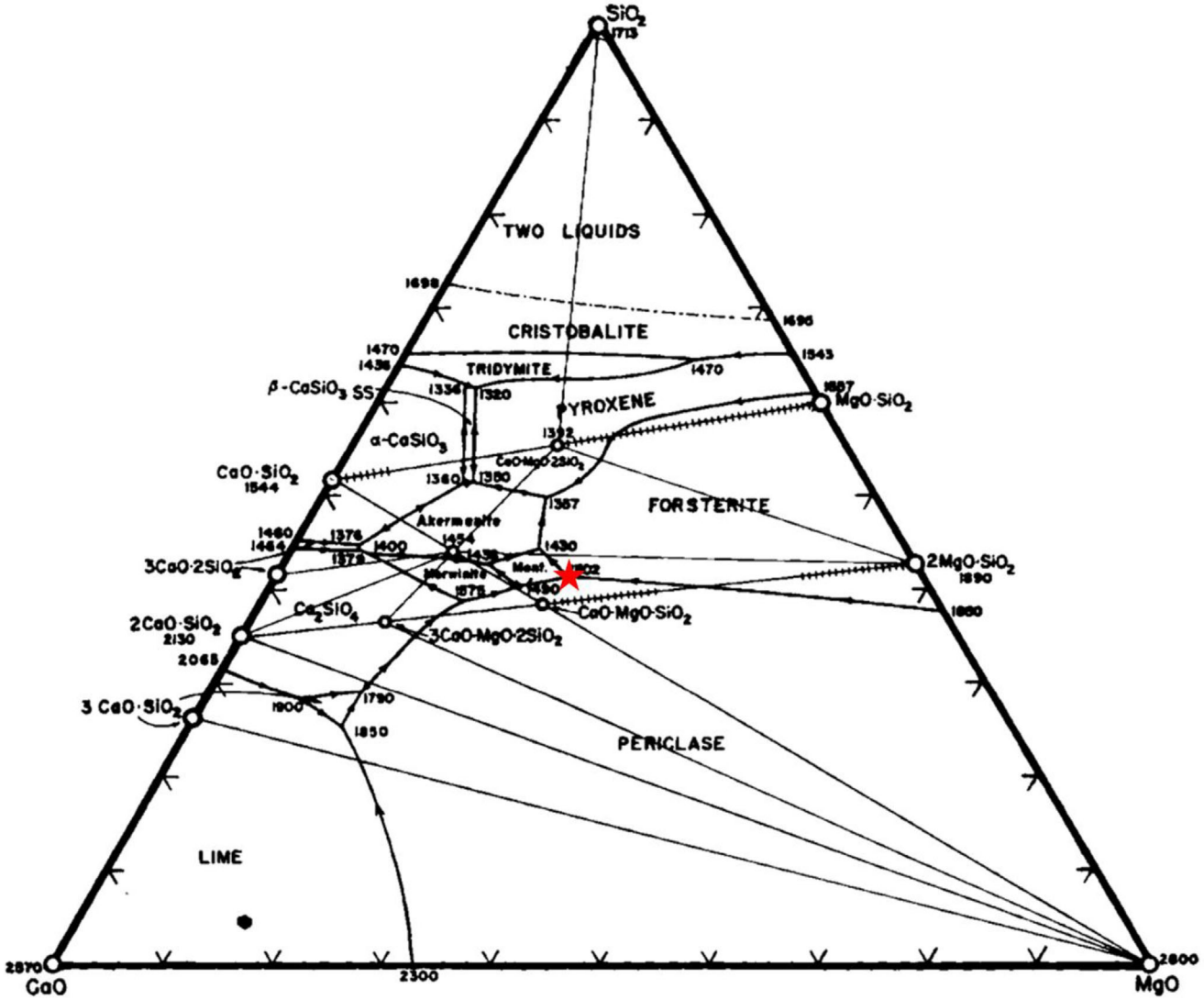

FIGURE 17 Phase diagram for the CaO-MgO-SiO_2 ternary system.[10] The star indicates the location of the invariant point for liquid + periclase → forsterite + monticellite at 1502°C.

and tundish cover flux, the flux can infiltrate into the refractory aggregates, forming a phase that may be corrosive to the MgO aggregate.[3] This has also been observed in postmortem analysis by the current authors,[9] where the secondary phases within the dead-burned magnesia aggregates was totally displaced by a calcium-aluminate liquid originating from the tundish cover flux. In such systems, merwinite may be observed in samples in addition to monticellite and forsterite. In addition to corrosion behavior, the liquid phase identified through confocal scanning laser microscopy may also influence the formation of magnesium aluminate spinel. In previous work by the current authors, it was observed that when tundish lining material is in contact with aluminum-killed steel, an accretion formed consisting of spinel and a liquid oxide phase. This liquid oxide phase was likely the result of the exudation of liquid from the refractory (possibly in addition to reoxidation of steel components), which provided a possible source of MgO that was more mobile than the MgO in the crystalline phase. Similarly, Kumar and Pistorius[13] observed that when melting aluminum-killed steel in two different MgO crucibles of varying purities, the crucible with a higher concentration of CaO-bearing impurities formed a slag layer, whereas the crucible with less CaO-bearing impurities only formed spinel at the steel/refractory interface. As a result, Mg transfer to the steel was 20 times higher in the slag-coated crucible than the spinel-coated crucible. While the slag layer observed in their work was different in chemistry than the liquid observed in the current work, it still indicates that a liquid oxide phase may contribute to the rate at which spinel builds on the surface of a refractory.

4 | CONCLUSIONS

Multiple dead-burned magnesia aggregates were heated up to 1550°C while being observed using a confocal scanning laser microscope. In each sample, a liquid was found to form between 1150 and 1350°C. This liquid forms from phases such as monticellite and forsterite, which bind the periclase crystallites together into larger aggregates. The behavior and predominance of this liquid is influenced by the concentration of these secondary phases, which are in turn influenced by the type of raw material used in the aggregate's manufacture. It is likely that impurities such as iron do play a role in driving down the melting temperature of these phases. The liquid generated exudes from the surface of the aggregate. In a steelmaking environment, such a liquid may interact with the steel melt or slag to detrimental effect, including the formation of spinel or corrosive liquids that infiltrate the refractory. Proposed future work includes conducting similar experiments with refractory aggregates in molten flux or steel to observe these specific interactions in situ.

REFERENCES

1. McDowell JS, Howe RM. Magnesite refractories. J Am Ceram Soc. 1920;3(3):185–246
2. Anderson O. Magnesia refractories in basic open-hearth steel furnaces. J Am Ceram Soc. 1934;17(8):221–35
3. Moshtaghioun BM, Monshi A. Hot corrosion mechanism of tundish plaster with steel slags in continuous casting. J Mater Sci. 2007;42:6720–8
4. Park JH. Formation mechanism of spinel-type inclusions in high-alloyed stainless steel melts. Metall Trans B. 2007;38(4):657–63
5. Park JH, Todoroki H. Control of $MgO{\cdot}Al_2O_3$ spinel inclusions in stainless steels. ISIJ Int. 2010;50(10):1333–46
6. Itoh H, Hino M, Ban-Ya S. Thermodynamics on the formation of spinel nonmetallic inclusions in liquid steel. Metall Trans B. 1997;28(5):953–6
7. Mantovani MC, Moraes LR, Leandro da Silva R, Cabral EF, Possente EA, Barbosa A, et al. Interactions between molten steel and different kinds of MgO based tundish linings. Ironmak Steelmak. 2013;40(5):319–25
8. Okuyama G, Yamaguchi K, Takeuchi S, Sorimachi KI. Effect of slag composition on the kinetics of formation of Al2O3-MgO inclusions in aluminum killed ferritic stainless steel. ISIJ Int. 2000;40(2):121–8
9. Richards T, Smith J, O'Malley R, Sander T. Comparison of two dry vibratable tundish linings through laboratory experiments. In: United International Technical Conference on Refractories; March 15–18, 2022; Chicago, USA
10. Ricker RW, Osborn EF. Additional phase equilibrium data for the system $CaO\text{-}MgO\text{-}SiO_2$. J Amer Ceram Soc. 1954;37(3):133–9
11. Biggar GM, O'Hara MJ. Melting of forsterite, monticellite, merwinite, spinel, and periclase assemblages. J Am Ceram Soc. 1970;53(10):534–7
12. Chuang HC, Hwang WS, Liu SH. Effects of basicity and FeO content on the softening and melting temperatures of the $CaO\text{-}SiO_2\text{-}MgO\text{-}Al_2O_3$ slag system. Mater Trans. 2009;50(6):1448–56
13. Kumar D, Pistorius PC. Rate of MgO pickup in alumina inclusions in aluminum-killed Steel. Metall Trans B. 2019;50(1):181–91

How to cite this article: Richards T, Athavale V, Smith J, O'Malley R. High temperature confocal scanning laser microscopy analysis of dead-burned magnesia aggregates. Int J Ceramic Eng Sci. 2023;1–14. https://doi.org/10.1002/ces2.10175